LA-UR -90-3383

CONF-910664--1

Los Alamos National Laboratory is operated by the University of California for the United States Department of Energy under contract W-7405-ENG-36

LA-UR--90-3383

DE91 002309

TITLE: A Three-Dimensional Free-Lagrange Code for Multimaterial Flow Simulations

AUTHOR(S): Manjit S. Sahota And Harold E. Trease

SUBMITTED TO: ASME-JSME 4th International Symposium on Liquid-Solid Flows

DISCLAIMER

Los Alamos National Laboratory
Los Alamos, New Mexico 87545

FORM NO 836 R4
ST NO 2629 5/81

A Three-Dimensional Free-Lagrange Code for Multimaterial Flow Simulations

by

Manjit S. Sahota and Harold E. Trease
Computational Physics Group
Applied Theoretical Physics Division
Los Alamos National Laboratory
Los Alamos, New Mexico

ABSTRACT

A time-dependent, three-dimensional, compressible, multicomponent, free-Lagrange code is currently under development at the Los Alamos National Laboratory. The code uses fixed-mass particles (called mass points) surrounded by median Lagrangian cells. These mass points are free to change their nearest-neighbor connections as they follow the fluid motion, which ensures accuracy in the differencing of equations and allows us to simulate flows with extreme distortions. All variables, including velocity, are mass-point centered, and time-advancement is performed using the finite-volume technique. The code conserves mass, momentum, and energy exactly, except in some pathological situations. We utilize the Voronoi connection algorithm for Delaunay tetrahedralization of the median mesh during mesh generations and mesh reconnections. The code is highly vectorized and utilizes all eight processors on a Cray YMP. Also, we have recently mapped the code to a massively parallel Connection Machine.

Some of the applications for the free-Lagrange method include atmospheric and ocean-circulation models, oil-reservoir and high-velocity impact simulations. These applications are in addition to our standard model problems of high-explosive driven shock-wave problems that involve high degree of deformation, shear flow, and turbulent mixing.

NOMENCLATURE

D/Dt	= substantial derivative, $\partial/\partial t + \vec{q}\cdot\nabla$, $1/s$
e	= specific total energy, J/kg
$\vec{f}$	= body-force vector per unit mass, N/kg
G	= shear modulus, N/m^2
I	= specific internal energy, J/kg
$\boldsymbol{I}$	= unit tensor
k	= thermal conductivity, $J/s-m-K$
p	= pressure, N/m^2
$\vec{q}$	= velocity vector, m/s
q'''	= heat-generation rate per unit volume, $J/s-m^3$
$\boldsymbol{S}$	= material-stress tensor, N/m^2
t	= time, s
T	= temperature, K
u,v,w	= coordinate velocities, m/s
x,y,z	= coordinate directions, m

Greek symbols

μ = fluid viscosity, including artificial viscosity, $kg/m-s$
ρ = density, kg/m^3
$\boldsymbol{\sigma}$ = overall stress tensor, including pressure, viscous-stress tensor, artificial-viscosity tensor, and material-stress tensor, N/m^2
$\boldsymbol{\tau}$ = viscous and artificial-viscosity stress tensor, N/m^2
$\vec{\omega}$ = vorticity vector, $\frac{1}{2}\nabla \times \vec{q}$, $1/m$

Subscripts

x,y,z = coordinate directions

Superscripts

* = transpose of a tensor

INTRODUCTION

Conventional Lagrangian methods have been proven to be very useful for solving the hydrodynamic equations, especially for problems requiring resolution of sharp fronts. These sharp fronts may be the result of shock waves in explosively-driven flows, saturation fronts encountered in oil-reservoir simulations, fronts associated with deformations and detached rings of the Gulf stream in ocean-acoustic applications, or material interfaces in gas-liquid-solid flow systems. The ability of the mesh to adapt to changing flow situations, and the absence of advection terms in the applicable differential equations because of mesh movement at the fluid velicity, render the Lagrangian methods far superior to the Eulerian techniques, both in terms of speed and accuracy. However, mesh-tangling in conventional Lagrangian methods has been such an impediment that it severly restricted the usefulness of the method for problems of practical import, except for one-dimensional flow situations.

Free-Lagrangian methods possess the same desirable features offered by the standard Lagrangian methods. However, mesh tangling is avoided because of the ability of the mesh to reconnect as it distorts. Of course, such reconnections reqire fluxing of the intensive variables through the mesh as fluid crosses the mesh boundaries. However, fluxing truncation errors due to differencing of equations are minimal because mesh reconnections occur only in regions of distortions.

We present a solution of the coupled hydrodynamic equations on a median mesh for a transient, three-dimensional, compressible, multimaterial, free-Lagrangian code. The solution algorithm uses fixed-mass particles (called mass points) that move at the fluid Lagrangian velocity and are surrounded by median Lagrangian cells constructed from Delaunay tetrahedra. These cells are free to change connectivity, which ensures accuracy in the differencing of equations and allows the code to handle extreme distortions. Details of the reconnection algorithm are provided by Fraser (1988), Marshall and Painter (1990), and Trease (1990). All variables are mass-point centered, and momentum and energy are conserved exactly except in some pathological situations. The Lagrangian nature of the median mesh makes fluxing through the mesh unnecessary except in the regions of reconnections.

A high-order finite-volume approximation has enabled us to successfully run several problems of interest on very coarse grids. A new artificial-viscosity formulation has allowed us to run most problems of interest in pure Lagrangian mode for the first half (or more) of the transients, thereby minimizing the fluxing errors caused by reconnections.

Currently, each computational cell represents a single phase and a single component, and interface between material boundaries is automatically tracked because of the Lagrangian nature of the mesh. All thermodynamic quantities at a given point in space are, therefore, unambiguously defined. Because phase change is allowed to take place in each computational cell, multiphase flow topologies are easily modeled for undispersed flows. However, the current algorithm is prohibitively expensive for modeling dispersed flows, because of the enormous number of single-phase single-component cells required. We will be implementing a mixed-cell model along with the solution of multiphase flow equations with associated interphasic exchange rates in the future.

THE MEDIAN MESH

Figure 1 shows the median mesh in two dimensions. The two-dimensional analogy

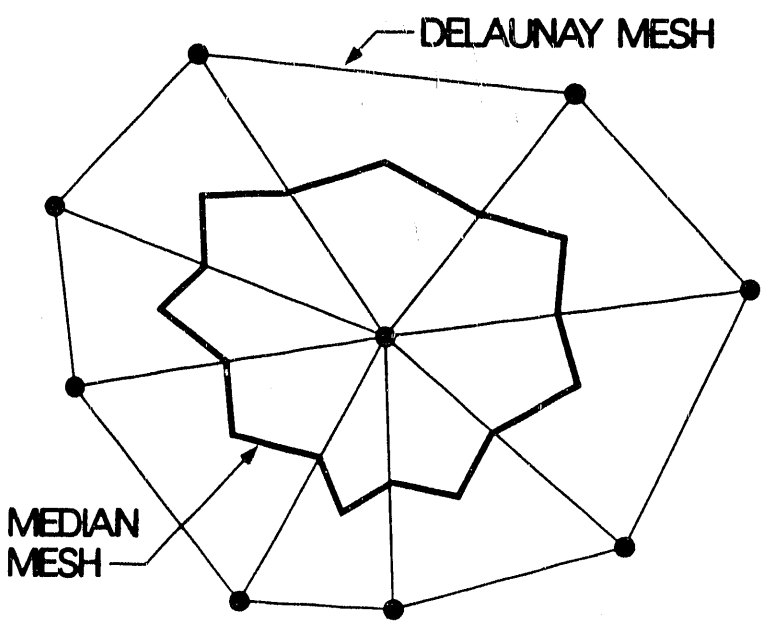

FIG. 1 Two-dimensional median mesh superimposed over the two-dimensional Delaunay mesh.

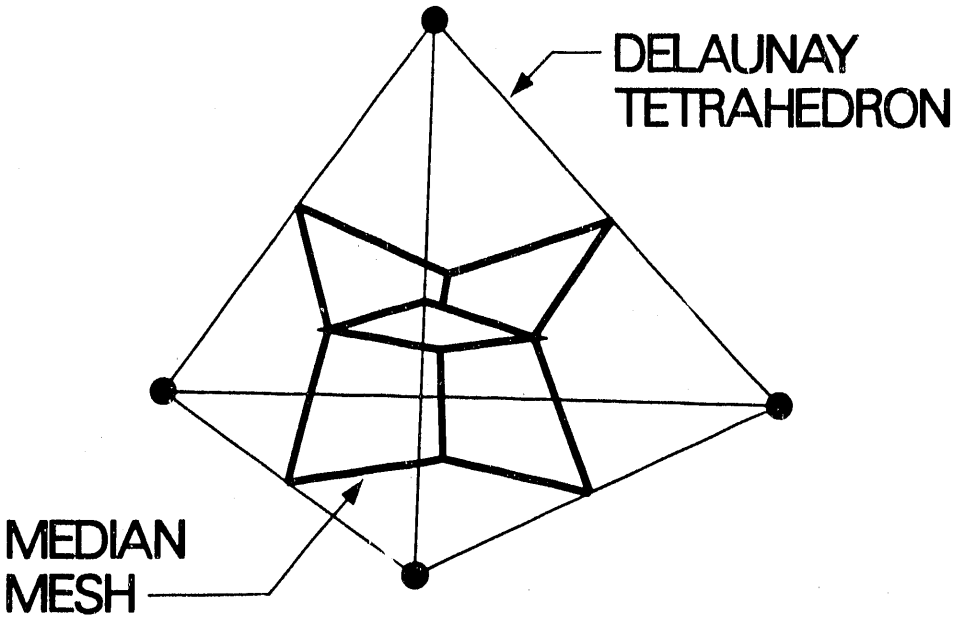

FIG. 2. Three-dimensional median mesh inside a Delaunay tetrahedron.

is used for easier comprehension. First we choose a nearest-neighbor set for each mass point in the mesh ensuring rigorous reciprocity (that is if mass point A is a neighbor of mass point B, then mass point B must also be a neighbor of mass point A). This set is defined by the Voronoi mesh. Then we construct the Delaunay triangles (tetrahedra in three dimensions) by connecting each mass point to its neighbors. This spans the entire space. Details of Delaunay tetrahedralization are provided by Sahota (1990b). The median mesh is then constructed by drawing a polygon around each mass point whose vertices are the area centroids and the connection midpoints. Because we always move the mass points at the Lagragian velocity, all the triangle (tetrahedron) verticies are Lagrangian. Therefore, the connection midpoints and the centroids also are Lagrangian. Thus the median-mesh boundaries move at the Lagrangian velocity and no fluxing is necessary due to the convective terms in the applicable differential equations. However, at the time of reconnections, the fluxing is required because the fluid crosses cell boundaries. It is clear from Fig. 1 that the median mesh with all variables centered at mass points is equivalent to a triangular (tetrahedral) Delaunay mesh with all variables defined at the triangle (tetrahedron) vertices.

The Delaunay triangles become Delaunay tetrahedra in three dimensions. Figure 2 shows a tetrahedron with median mesh superimposed over it. The three-dimensional median mesh is drawn by connecting each connection midpoint to its two adjacent face centroids, which are then connected to the tetrahedron centroid. This results in the tetrahedron volume being shared equally among the four mass points. Again, since the mass points are Lagrangian; the connection midpoints, the face centroids, and the tetrahedron centroid are Lagrangian. Therefore, the boundaries of the three-dimensional median mesh are Lagrangian.

To enhance computational efficiency, all hydrodynamic calculations are done at a tetrahedron level in super-vector loops, and contributions to accelerations from each tetrahedron are accumulated (through indirect addressing) at each of the four mass points adjoining the tetrahedron. This procedure is computationally more efficient than looping over the

mass points, because a tetrahedron is computed only once even though it is shared by four mass points.

GOVERNING EQUATIONS

The hydrodynamic equations solved are the mass, momentum, and total energy equations. The internal energy is calculated by subtracting the kinetic energy from the total energy. These equations are given below.

Mass

$$\frac{D\rho}{Dt} = -\rho \nabla \cdot \vec{q} \quad . \tag{1}$$

Momentum

$$\rho \frac{D\vec{q}}{Dt} = \nabla \cdot \boldsymbol{\sigma} + \rho \vec{f} \quad , \tag{2}$$

where the stress tensor, $\boldsymbol{\sigma}$, is defined as,

$$\boldsymbol{\sigma} = -p\boldsymbol{I} + \boldsymbol{\tau} + \boldsymbol{S} \quad , \tag{3}$$

where the viscous-stress tensor, $\boldsymbol{\tau}$, is defined as

$$\boldsymbol{\tau} = \mu \begin{pmatrix} 2(\frac{\partial u}{\partial x} - \frac{1}{3}\nabla \cdot \vec{q}) & \frac{\partial u}{\partial y} + \frac{\partial v}{\partial x} & \frac{\partial u}{\partial z} + \frac{\partial w}{\partial x} \\ \frac{\partial v}{\partial x} + \frac{\partial u}{\partial y} & 2(\frac{\partial v}{\partial y} - \frac{1}{3}\nabla \cdot \vec{q}) & \frac{\partial v}{\partial z} + \frac{\partial w}{\partial y} \\ \frac{\partial w}{\partial x} + \frac{\partial u}{\partial z} & \frac{\partial w}{\partial y} + \frac{\partial v}{\partial z} & 2(\frac{\partial w}{\partial z} - \frac{1}{3}\nabla \cdot \vec{q}) \end{pmatrix} \quad , \tag{4}$$

and the material-stress-deviator, $\boldsymbol{S}$, is calculated from

$$\frac{D\boldsymbol{S}}{Dt} = \frac{G}{\mu}\boldsymbol{\tau} + \vec{\omega} \times \boldsymbol{S} + (\vec{\omega} \times \boldsymbol{S})^{\star} \quad , \tag{5}$$

where the vorticity terms (terms containing $\vec{\omega}$) represent the rigid-body rotation. The vorticity vector, $\vec{\omega}$, is defined as

$$\vec{\omega} = \frac{1}{2}\nabla \times \vec{q} = \frac{1}{2}\begin{pmatrix} \frac{\partial w}{\partial y} - \frac{\partial v}{\partial z} \\ \frac{\partial u}{\partial z} - \frac{\partial w}{\partial x} \\ \frac{\partial v}{\partial x} - \frac{\partial u}{\partial y} \end{pmatrix} \quad . \tag{6}$$

Total energy

$$\rho \frac{De}{Dt} = \nabla \cdot (\boldsymbol{\sigma} \cdot \vec{q}) + \nabla \cdot (k\nabla T) + \rho \vec{f} \cdot \vec{q} + q''' \quad . \tag{7}$$

To obtain closure, we need an equation-of-state, which follows.

$$p = p(\rho, I) \quad . \tag{8}$$

NUMERICAL METHOD

Because the computations are done on a Lagrangian mesh, equation (1) is trival to solve, i.e., the density is calculated by dividing mass by volume. The momentum and energy equations are solved by integrating them over cells and applying the divergence theorem. The stress-deviator equations (5) are solved similarly. Currently, all time-advancements are carried out in an explicit manner except for $\nabla \cdot (k \nabla T)$ term in the energy equation, which is evaluated following a hybrid explicit-implicit technique (Sahota, 1990a).

A single-step time advancement of equations (2) and (7) using the old-time values of $\boldsymbol{\sigma}$ and $\vec{q}$ is known to be unstable without the use of a linear artificial viscosity (in addition to quadratic artificial viscosity). However, stability can be achieved by computing $\boldsymbol{\sigma}$ and $\vec{q}$ in the middle of a time cycle, without the use of linear-artificial viscosity. This approach also makes the time advancement second-order accurate. Details of the numerical method are provided by Sahota (1989, 1990a).

RESULTS

Calculated density profiles for the infinite spherical shock explosion problem of Noh (1985) are compared with the analytic result in Fig. 3 at 0.6 μs. The calculations were done

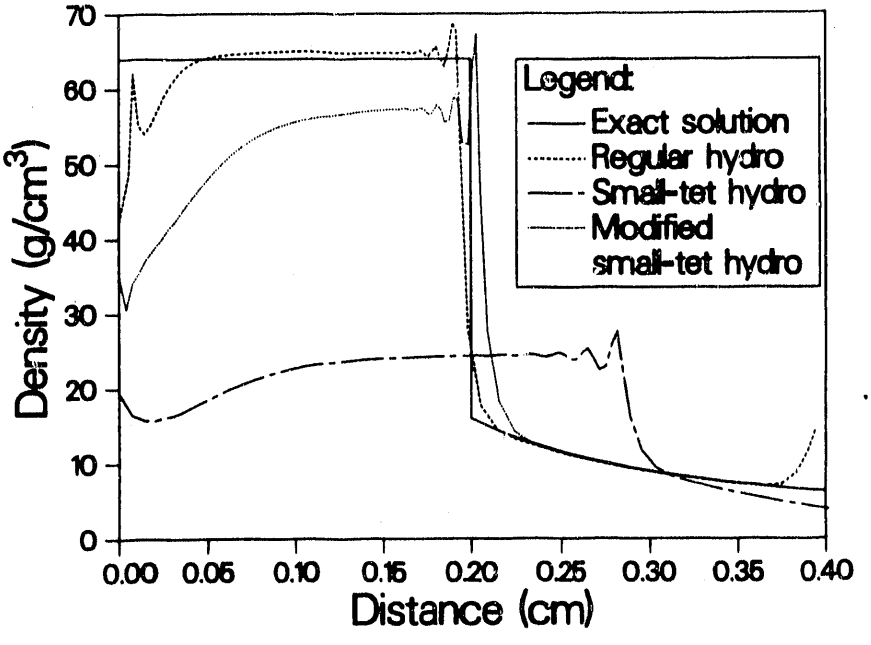

FIG. 3. Comparison of the calculated density profiles with the exact solution for the spherical Noh (1985) problem at 0.6 μs.

on a row of 100 points surrounded by a 40-degree cone of reflective boundaries represented by four rows of 50 points each. The figure shows two calculations. The first calculation was done using the proposed free-Lagrange technique. The second calculation was done using a conventional artificial-viscosity approach typically used in two-dimensional codes with success. The comparison between the proposed technique and analytic result is excellent. However, conventional artificial-viscosity calculation is far inferior upstream of the shock, and unacceptable downstream of the shock, with a peak density of only $\sim 24 g/cm^3$. This gross error is the combined result of a spring-type artificial viscosity and coarse angular zoning (20-degree zoning), which is typically the case in three dimensions. The conventional

artificial-viscosity form does not recognize the mass points approaching each other due to physical spherical convergence; and due to large angular zoning, the artificial viscosity exerts a large repulsive force that tends to destroy the compression process. This is a first-order error in space and its effect disappears as the angular zoning becomes finer. We use a traceless form of the tensor artificial viscosity that does not result in anomalous repulsive forces (Sahota, 1989).

One of our primary concerns was that, since we could not generate symmetric meshes in three dimensions, how symmetric our predictions would be for physically symmetric problems? Figure (4) shows a fully three-dimensional calculation for the Noh problem with

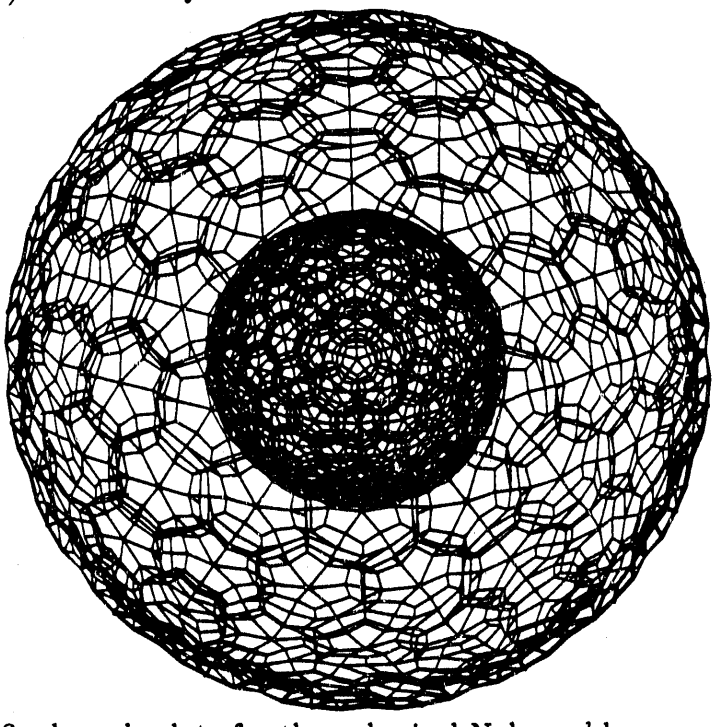

FIG. 4. Initial and final mesh plots for the spherical Noh problem computed on an asymmetric three-dimensional mesh.

initial and final mesh configurations superimposed over each other. Clearly, the problem stays symmetric. We also have performed calculations for a spherically expanding wave under an initially uniform pressure, and have simulated several other spherically symmetric problems, which also stay symmetric on asymmetic meshes.

Figure (5) shows a comparison of the experimental and calculated interface growth rates for the shock-tube experiment of Andronov *et al.* (1976). The instability was initiated by propagating a weak shock through a perturbed interface between two fluids at different densities. The calculation and the data agree within $\sim$ 10%. The calculation also compares favorably with Youngs' (1984) two-dimensional calculation of single-wavelength perturbation (not shown). Figure (6) shows the calculated instability in the heavier fluid at 1 ms.

To test the material-strength model, we simulated a strength-dominated vibrating-shell problem, whereby a perfectly-elastic spherical shell is given an initial radially inward velocity and is allowed to vibrate. Figure (7) shows the radial position of a point as a function of time. The calculated time period of 28.8μs matches favorably with an analytic value of $\sim 28\mu s$.

The free-Lagrangian algorithm is capable of modeling a wide range of physics problems.

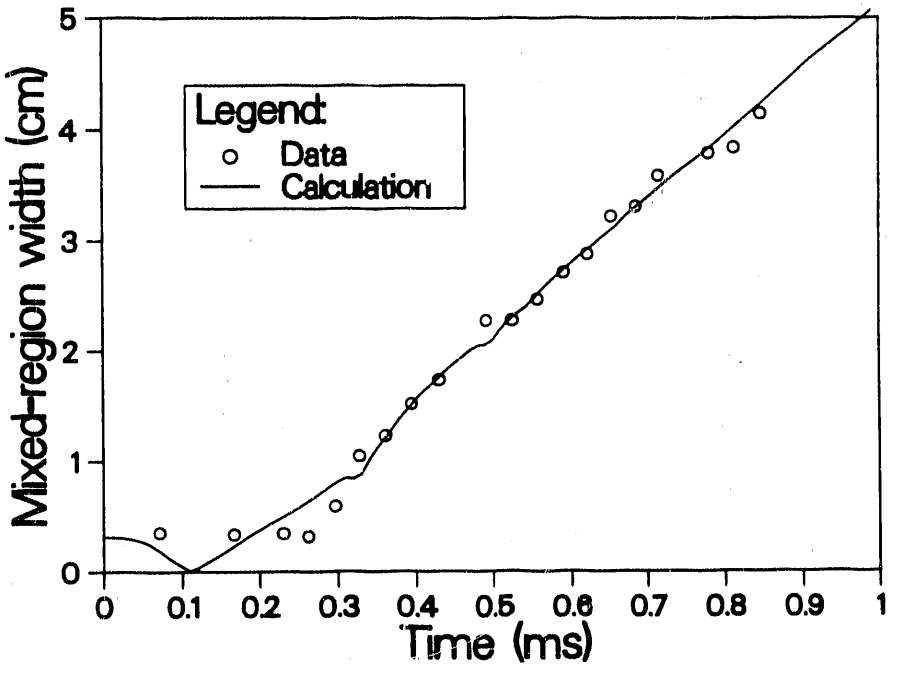

FIG. 5. Comparison of the experimental and predicted mixed-region growth histories for the shock-tube experiment of Andronov *et al.* (1976). The time is measured from arrival of the first shock at the interface.

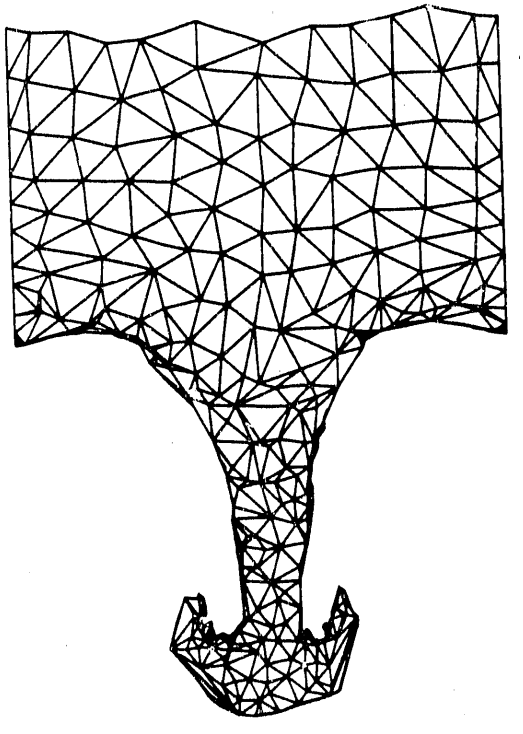

FIG. 6. Computed instability for the shock-tube experiment at 1 *ms*.

The previous examples demonstrate how well we simulate shock-driven fluid flow problems. Figures 8-10 show the development of a metal jet from a shape-charge calculation. In this

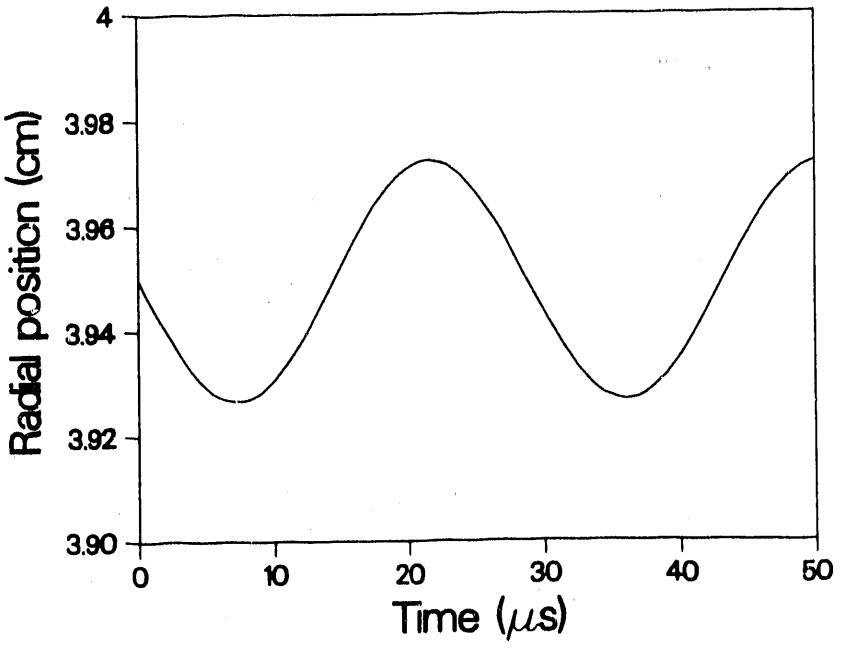

FIG. 7. Calculated radial-position history of a point for the vibrating-shell problem.

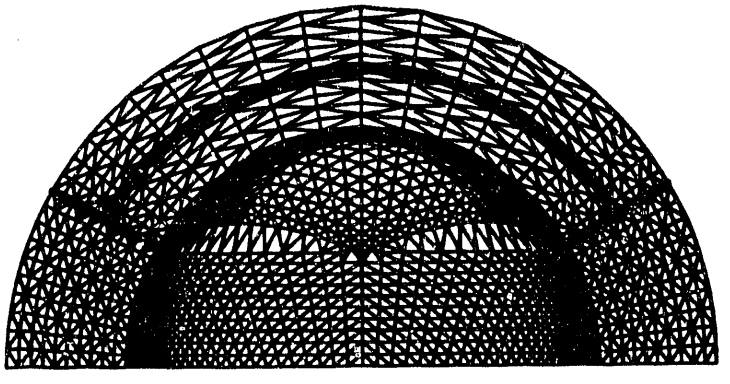

FIG. 8. Initial mesh plot for a shape charge.

calculation the jet is made of aluminum, the back plate is made of copper with a charge of high explosive between them. The high explosive is detonated at one point on axis at the interface between the copper and the high explosive. The copper is not axisymmetric about the center line of the shape charge, but has been formed into a square shape. This makes the calculation three-dimensional. The result of this square piece of copper is to produce an aluminum jet that is square, but the corners are 90 degrees out of phase with respect to the corners of the original piece of copper. This process can be clearly observed in a movie of the calculation.

We are exploring the feasibility of using the free-Lagrange technique for global atmospheric and ocean-circulation modeling. Figure 11 shows the free-Lagrange mesh structure at the surface of the earth. These surface triangles form the bases of tetrahedra that

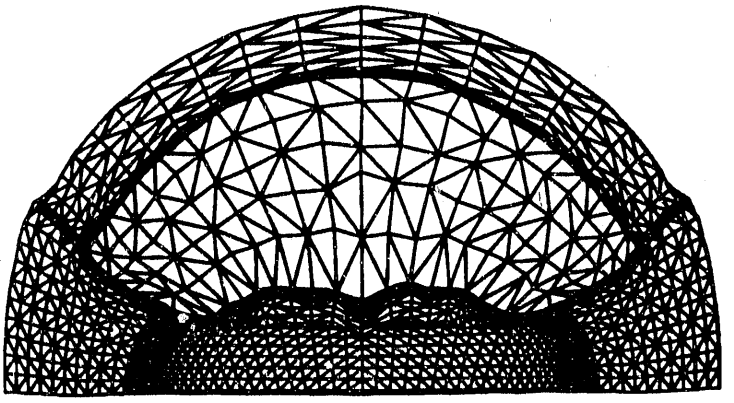

FIG. 9. Formation of aluminum jet for a shape charge at 11.5 μs.

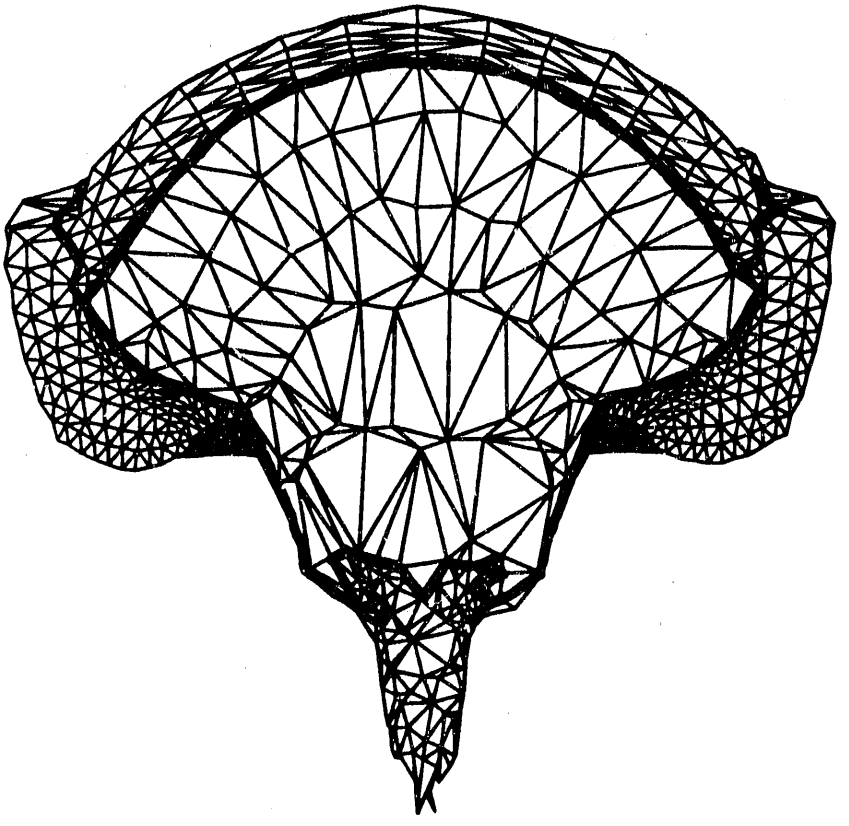

FIG. 10. Formation of aluminum jet for a shape charge at 27.0 μs.

extend up through the atmosphere to the next layer of mesh points. In this example we have twenty vertical layers of points. It can be noted that points are placed on the earth's surface such that they map the topography. Here we see that the land masses and the oceans have been zoned with different amounts of resolution. This demonstrates the static, variable zoning capability that the unstructured grid provides. We also can dynamically add and remove mesh resolution by comparing locally the length scales resolved by the mesh and the physical length scales determined from spacial gradient information. If these

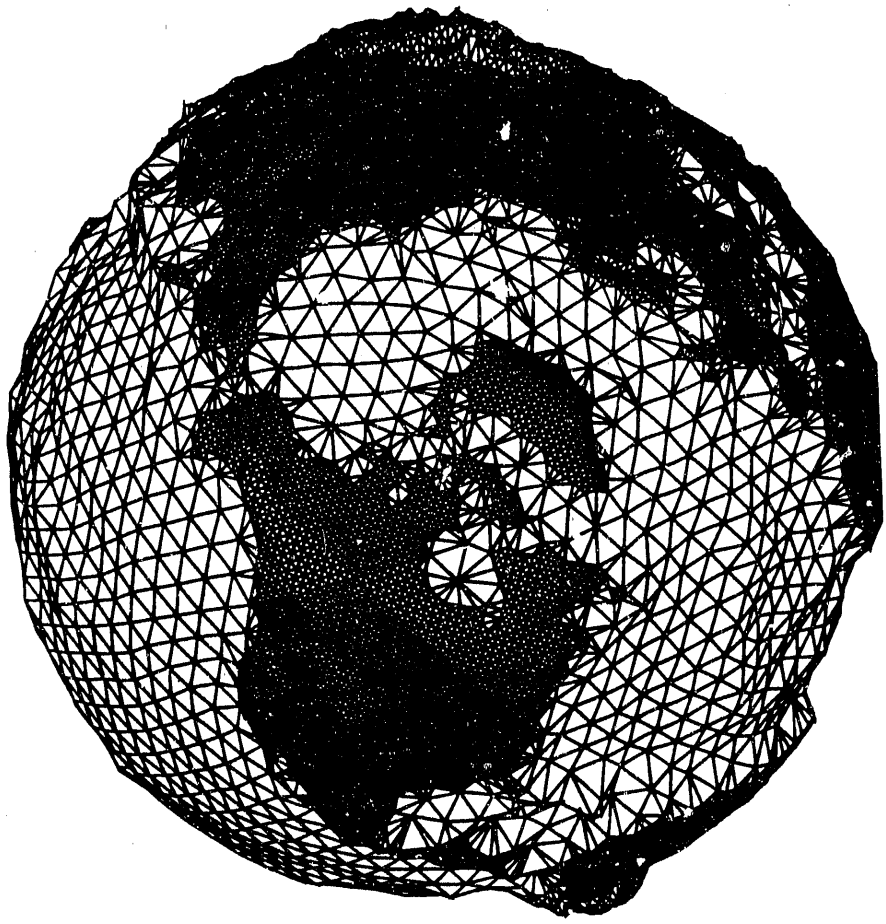

FIG. 11. Mesh plot of earth showing variable-zoning capability of the free-Lagrange method.

length scales differ by too large a factor then the code will automatically add or remove resolution. A good example of this process occurs when a tropical cyclone forms. The code will detect the lack of resolution to resolve vorticity near the source of the cyclone and will automarically add more zones. This process continues until the cyclone starts to dissipate, then mesh resolution will be removed automatically by the code. Figure 12 is an example of the wind shear at the surface of the earth.

CONCLUSIONS

The free-Lagrangian methods provide the accuracy of standard Lagrangian approaches and the robustness of Eulerian approaches because of the ability of the mesh to reconnect. Because the mesh is not allowed to distort, the finite-volume truncation errors are expected to be even lower than the Lagrangian methods for complex flow situations. The method presented uses a completely unstructured grid, and as a result, the technique is inherently adaptable to arbitrary geometries and flow structures. Because this mesh adaptability allows the use of much fewer grid points for equivalent accuracy, far better computational efficiency than the structured mesh schemes is obtained for complex geometries. Because of its Lagrangian nature, the free-Lagrange method introduces no artificial diffusion due to advective terms in the differential equations. This lack of artificial diffusion leads to far better accuracy in handling high-shear flows as compared to standard Eulerian approaches.

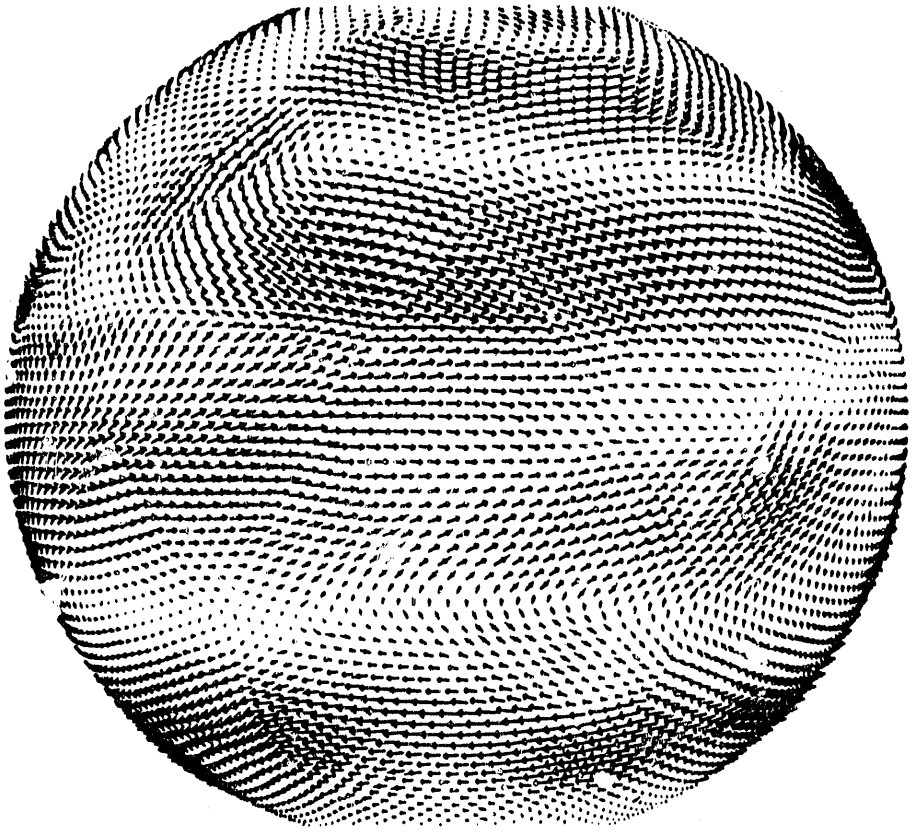

FIG. 12. Calculated wind-shear pattern for atmospheric circulation model.

The results presented for several problems of interest are very encouraging. We also have performed several other calculations of interest that compare very favorably with the analytic results and the experimental data. We had recognized from the start that we could not generate perfectly symmetric meshes in three dimensions. In spite of our inablity to generate symmetric meshes, we have found that we are able to calculate symmetric results for physically symmetric problems even on comparatively coarser grids compared to the grids conventionally used in two-dimensional simulations.

We use a tetrahedron-centered traceless form of tensor artificial viscosity (Sahota, 1989), which has eliminated anomalous repulsive forces among mass points in spherically converging geometries. We have been able to run problems with tetrahedron aspect ratios of several hundred to one.

The free-Lagrange algorithm was parallelized on the Cray family of supercomputers since its inception, and has been recently mapped onto the massively parallel Connection Machine (CM-2). In spite of its unstructured grid, the algorithm is naturally amenable to massively parallel architectures by collecting tetrahedron-related data and assigning each tetrahedron to a virtual processor.

We also are investigating the applicability of the free-Lagrange method to oil-reservoir simulations, because of its ability to resolve saturation (sharp) fronts encountered in such

applications. This would, of course, require implicitizing more terms in the applicable differential equations (especially the pressure), and explicitly using the multiphase multicomponent formulations with a mixed-cell treatment, and replacing the momentum equation with Darcy's law (a simplification).

ACKNOWLEDGEMENTS

This work was performed under the auspices of the U.S. Department of Energy by the Los Alamos National Laboratory under Contract W-7405-ENG-36. We thank Jim Painter, Jean Marshall, and John Fowler for calculational assistance.

REFERENCES

Andronov, V., Bakhrakh, S. M., Meshkov, E. E., Mokhov, V. N., Nikiforov, V. V., Pevnitskii, A. V., and Tolshmyakov, A. I., 1976, *Soviet Physics*, JETP, No. 44, pp 424–427.

Fraser, D. M., 1988, "Tetrahedral Meshing Considerations for a Three-Dimension Free-Lagrangian Code." Los Alamos National Laboratory report, LA-UR-88-3707.

Marshall, J. C., and Painter, J. W., 1990, "Reconnection and Fluxing Algorithms in a Three-Dimensional Free-Lagrangian Hydrocode," Proceedings of the Next Free-Lagrange Conference, Jackson Lake Lodge, Wyoming, June 3-7, 1990, Springer-Verlag Press, to be published.

Noh, W. F., 1985, "Errors for Calculations of Strong Shocks Using an Artificial Viscosity and an Artificial Heat Flux," Lawrence Livermore National Laboratory report UCRL-53669.

Sahota, M. S., 1989, "Three-Dimensional Free-Lagrangian Hydrodynamics," Los Alamos National Laboratory report, LA-UR-89-11-79.

Sahota, M. S., 1990a, "An Explicit-Implicit Solution of the Hydrodynamic and Radiation Equations," Proceedings of the Next Free-Lagrange Conference, Jackson Lake Lodge, Wyoming, June 3-7, 1990, Springer-Verlag Press, to be published.

Sahota, M. S., 1990b, "Delaunay Tetrahedralization in a Three-Dimensional Free-Lagrangian Multimaterial Code," Proceedings of the Next Free-Lagrange Conference, Jackson Lake Lodge, Wyoming, June 3-7, 1990, Springer-Verlag Press, to be published.

Trease, H. E., 1990, "Mesh Reconnection on a Massively Parallel computer," Proceedings of the Next Free-Lagrange Conference, Jackson Lake Lodge, Wyoming, June 3-7, 1990, Springer-Verlag Press, to be published.

Youngs, D. L., 1984, "Numerical Simulation of Turbulent Mixing by Rayleigh-Taylor Instability," *Physica*, Vol. 12D, pp 32–44.

END

DATE FILMED

05 / 08 / 91